HEFAT2010
7th International Conference on Heat Transfer, Fluid Mechanics and Thermodynamics
19-21 July 2010
Antalya, Turkey

INVESTIGATION OF THE FLOW STRUCTURE OVER A NONSLENDER DELTA WING: EFFECT OF YAW ANGLE

Canpolat C.*, Sahin B., Yayla S. and Akilli H.
*Author for correspondence
Department of Mechanical Engineering,
University of Cukurova,
Adana,01330,
Turkey,
E-mail: ccanpolat@cu.edu.tr

ABSTRACT

In the present work, vortical flow structure of a delta wing of low sweep angle ($\Lambda=40^o$) was investigated both qualitatively and quantitatively using dye visualization and stereoscopic Particle Image Velicimetry (sPIV) technique. Firstly, the leading edge vortex formation is observed using the dye visualization technique by varying angle of attack within the range of $7^o \leq \alpha \leq 17^o$ and yaw angle $0^o \leq \theta \leq 15^o$. Secondly, changes in flow structure were observed by varying the yaw angle of the delta wing within the range of $0^o \leq \theta \leq 15^o$ for the angle of attack of $\alpha=10°$.

The dye visualization experiments were conducted for investigating the flow structure over the wing qualitatively in the plan-view plane. From PIV experiments, patterns of time-averaged vorticity, $\langle\omega\rangle$, streamline, $\langle\Psi\rangle$ distribution of velocity vectors,$\langle V\rangle$ and transverse, $\langle v\rangle/U$ and streamwise, $\langle u\rangle/U$ velocity components and Reynolds stress correlations, $\langle u'v'\rangle/U^2$ for various angles of attack and yaw angles were obtained in order to reveal the flow mechanism in plan-view plane adjacent to the surface of the wing.

INTRODUCTION

Delta wings are used in various types of airplanes employed in different types of missions. Therefore, delta planform is substantially important in aerodynamic configuration. Delta wings having low sweep angle (nonslender) are often used for unmanned and micro air vehicle [(UAV) and (MAV)] configurations.

In three dimensional flows, boundary layer separation leads to the formation of vortical structures formed by rolling up of viscous flow sheet, previously confined in a thin layer attached to the wall, which suddenly springs into the outer non-dissipative flow. Such vortices appear in a large number of circumstances and they often play a dominant role in the overall flow properties [1]. In the case of flow over delta wing, separation is occurred due to the effect of angle of attack and the sharp edge of the delta wing which causes a pair of coherent leading edge vortices. These vortices could not maintain their strength along their central axes and vortex breakdown is occurred at a certain distance from delta wing apex when angle of attack is increased slightly.

Yaniktepe and Rockwell [4]aimed to investigate the unresolved concepts such as averaged structure of shear layer from leading edge of wing, unsteady features of separated layer adjacent to surface of the wing, control of the flow structure by leading edge perturbations using PIV and appropriate processing of selected and cinema sequences of images. They mainly focused on the crossflow planes, where vortex breakdown and stall phenomena occur. It was concluded that the flow structure on a (nonslender) delta wing of low sweep angle exhibits a number of distinctive characteristics compared with slender delta wings. In addition to the previous work, Yaniktepe and Rockwell [3] characterized the instantaneous and averaged flow structure on diamond and lambda planforms using PIV. They focused on the structure in the trailing-edge region, over a range of angle of attack. It is reported that the abrupt change in sweep angle, which is characteristic of both diamond and lambda planforms, along with the different trailing edge configurations of these planforms, yields distinctive features of the patterns, relative to the case of a simple delta wing. Yavuz et al. [4] studied the near-surface vortical flow structure of the nonslender delta wing having sweep angle of $\Lambda=38.7^o$ using PIV. In other words, they aimed at presenting the vortical flow structure regions of vortex breakdown occurred above its surface. They explained the near surface topology of the nonslender delta wing based on the time-averaged and instantaneous streamlines, vorticity patterns and patterns of the time-averaged component of both transverse and streamwise velocity. Ol and Gharib [5] experimentally investigated the onset of vortex breakdown over delta wings having sweep angle of $\Lambda= 50°$ and $65°$ by using dye visualization and the stereo PIV technique. Various features of

the leading edge vortex including a large-scale collapse of the rolled-up were demonstrated. Elkhoury and Rockwell [6] provided various measurements of the visualized dye patterns including the degree of interaction of vortices, the onset of vortex breakdown, and effective sweep angle of the wing root vortex. Taylor and Gursul [7] aimed at presenting the results of an experimental study into the characteristics of unsteady vortex flows and buffeting of a wing with 50° leading edge sweep angle using PIV and Laser Doppler Velocimetry (LDV), the surface flow visualization, force balance measurement and wing-tip acceleration measurement. Gursul et al. [8] reviewed unsteady aerodynamics of nonslender delta wings, covering topics of shear layer instabilities, structure of nonslender vortices, breakdown, maneuvering wings, and fluid/structure interactions. Elkhoury et al. [9] investigated the Reynolds number dependence of the near-surface flow structure and topology on a representative UCAV planform using PIV, in order to complement classical dye visualization. Goruney and Rockwell [10] characterized the near-surface flow structure and topology on a delta wing of moderate sweep angle which are intimately related to the onset and development of flow separation, and the possibility of mitigation or elimination of points of surface separation via sinusoidal leading edges. A technique of stereoscopic PIV allows interpretation of the near-surface topology and associate critical points, in conjunction with surface normal velocity and vorticity. However, the disorganization and complexity of the flow structure is increased after occurrence of the vortex breakdown when yaw angle becomes effective on the flow structure over delta wing. Sohn et al. [11] visually investigated the development and interaction of vortices in cross-flow planes at various locations on the delta wing with leading edge extension (LEX) using micro water droplets and a laser beam sheet. The range of attack angle was taken as $12^o \leq \alpha \leq 24^o$ at yaw angles of 0^o,-5^o and -10^o. In general, when the angle of attack increases the wing vortex and LEX vortex coiled around with higher strength and the cores of this combined vortices shifted inboard and upward. It was indicated that introducing yaw angle the coiling, the merging and diffusion of the wing and LEX vortices increased on the windward side, whereas they become delayed significantly on the leeward side. Their study confirmed that the yaw angle has a profound effect on the vortex structures. In addition Sohn and Lee [12,13], Lee and Sohn [14] also observed the effect of the yaw angle on the flow structure over the delta wing. Finally, Canpolat et al. [15] investigated the formation and development of leading edge vortices, vortex breakdown, three dimensional separation and disorganized flow structure over the delta wing which has a leading edge sweep angle of $\Lambda=40^o$ varying angle of attack within the range of $7^o \leq \alpha \leq 17^o$ and varying the yaw angle of the delta wing within the range of $0^o \leq \theta \leq 15^o$ by using the dye visualization technique.

NOMENCLATURE

α		Angle of attack
θ		Yaw angle
Λ		Sweep angle
C	[m]	Chord of delta wing
Re_c		Reynolds number according to the delta wing chord length
$<\Psi>$		Ttime-averaged streamline
$<V>$		Time-averaged velocity vectors
$<v>/U$		Ttime-averaged components of streamwise velocity
$<u>/U$		Time-averaged components of transverse velocity
$\Delta[<u'v'>/U^2$		Time-averaged turbulent Reynolds stress components

EXPERIMENTAL ARRANGEMENTS AND INSTRUMENTATIONS

Experiments were conducted on a circulating free-surface water channel. The internal dimensions of the water channel were of 8000 mm × 1000 mm × 750 mm which was made from 15 mm thick transparent Plexiglas sheet with upstream and downstream fiberglass reservoirs. Before reaching the test chamber, the water was pumped into a settling chamber and passed through a honeycomb section and a 2:1 channel contraction. The delta wing has a chord length of C=101mm for PIV experiments and C=140mm for dye experiments with a sweep angle of $\Lambda=40^o$. The schematic of experimental arrangement is presented in Figure 1.The depth of the water in the test section was adjusted to 530 mm for the present experiments. The Reynolds number based on the delta wing chord was kept constant for all experiments as $Re_c=10000$ which corresponds to the free-stream velocity of 97 mm/s for PIV experiments and 72 mm/s for dye experiments.

A fluorescent dye which shines under the laser sheet was used to create color change in the water to visualize flow characteristics over the delta wing during the dye experiments. Dye was injected the near field of the delta wing trailing edge by plastic pipe and dye was passed through a narrow and close channel in the delta wing to its apex. The video camera (SONY HD-SR1) was used to capture the instantaneous video images of the vortex flow structures. For the present investigation, the flow characteristics over the delta wing in the plan-view plane was presented for angle of attack α =7°, 10°, 13°, 17° and yaw angles such as θ= 0° and 10° for all dye experiments.

Instantaneous velocity vectors were measured in a region illuminated by a two-dimensional laser sheet by using the Stereo PIV technique which allows performing three dimensional measurements on two dimensional plane. Emphasis on this technique is the capability of looking at the measuring plane by two cameras with same angle from the horizontal plane based on the principle of stereoscopic imaging which is the same with the human eyesight. Prasad [16] declared that all stereoscopic systems, despite the wide variety in configurations, must satisfy the basic requirements of recording two simultaneous, but different views of same object. The two views are then combined using one of an assortment of algorithms to reconstruct the three-dimensional field. The detailed information about Stereoscopic PIV could be obtained from Prasad [16], Adrian [17], Raffel et al. [18].

Velocity vector measurements were performed by a Dantec stereoscopic PIV system. The flow field illumination was provided by two Nd:Yag pulsed laser sources of a wavelength of 532 nm, each with a maximum energy output of 120 mJ. Dantec Flow Map Processor which controlled the timing of the data acquisition was used for synchronizing the camera and laser units. The movements of the particles were recorded using a CCD camera with a resolution of 1600 x 1186

pixels. The camera was equipped with a 60 mm focal-length lens. Totally 900 instantaneous images were taken with an acquisition frequency of 15 Hz for each continuous run. Dantec digital PIV software employing frame-to-frame adaptive correlation technique was used to calculate the raw displacement vector field from instantaneous images of measuring field. In the image processing, 32 x 32 pixels with rectangular effective interrogation windows was used. During the interrogation process, an overlap of 50% was employed in order to satisfy Nyquist criterion. For the present investigation, the stereoscopic PIV experiments were conducted for single crossflow plane (plan-view). In this paper, the flow characteristics over the delta wing in plan-view plane is presented for both angle of attack and yaw angles of α =10° ; θ= 0°, 6°, 8°, 15° for stereoscopic PIV experiments.

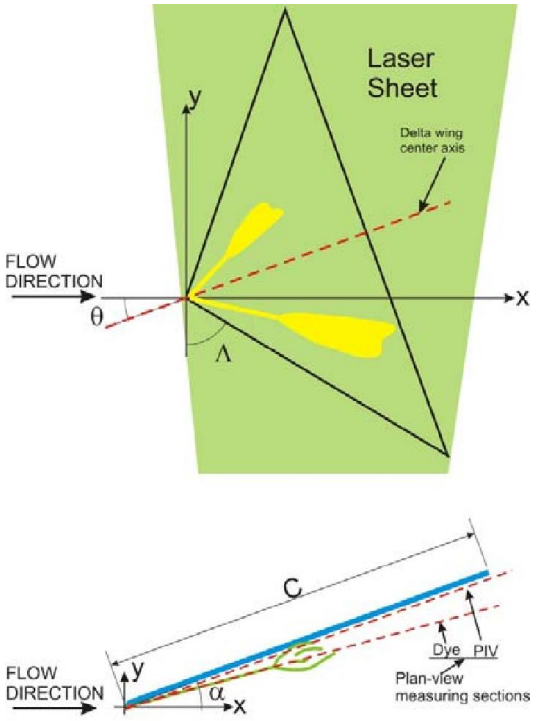

Figure 1 The schematic of experimental arrangement

RESULTS AND DISCUSSIONS

1. Dye Visualization Results

Examining all dye experiments, a coherent leading edge vortices emanating from the leading edge of the delta wing are clearly identifiable and vortex breakdowns occur after a certain distance from the delta wing apex as seen in Figure 2. These leading edge vortices develop at very low angles of attack and form close to the wing surface for nonslender delta wings as also stated by Gursul et al.[8]. Symmetrical flow structure occupies the whole wing in the case of zero yaw angle. The location of vortex breakdown moves towards to the apex of the delta wing rapidly when the angle of attack increases slightly. However, locations of vortex breakdown move upstream-downstream directions through its central axis. A large-scale separation/stall was observed over the entire of the surface of the wing when the angle of attack is increased.

When the yaw angle becomes effective, the flow structure on the both side of the delta wing deteriorated. In other words, symmetrical flow structure over the delta wing is not maintained with increasing the value of yaw angle. The location of vortex breakdown on the leeward side of the delta wing begins to delay compared to the windward side of the delta wing which is the wing side that leading into the flow (windward side) with decreasing effect of sweep angle when the delta wing was under effect of the yaw angle. The secondary vortex next to the leading edge vortex appears at yaw angles of θ=8°, 10° and 15° for the angle of attack, α=7°. As stated by Canpolat et al. [15], the yaw angle become effective on the flow structure over the delta wing beyond the value of θ=6° which means the flow structure over the delta wing was nearly symmetric up to this value.

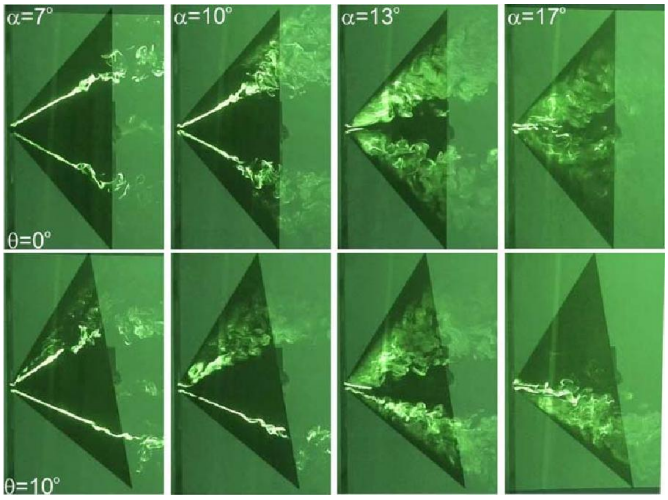

Figure 2 Formation and development of the leading edge vortex and vortex breakdown

There was an interesting event when the angle of attack was set to α=10° and yaw angle θ=10° as seen from Figure 3. A swirling-type vortex was occurred next to the leading edge vortex close to wing apex. On the upper region of the mid-cord axis of the delta wing, a separated flow takes place at $\theta \geq 10°$ along the windward side of the delta wing. No more leading edge vortex is developed over the delta wing at the windward side for all cases of yaw angle when the angle of attack is increased to higher values. Extensive information about results of dye visualization experiments could be obtained from Canpolat et al. [15].

2. Stereoscopic Particle Image Velocimetry Results

a. Patterns of Time-Averaged Velocity Vectors, <V> and Streamlines, <Ψ>

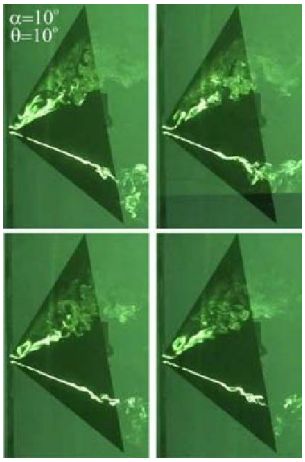

Figure 3 Formation and development of the swirling-type vortex, leading edge vortex and vortex breakdown

Patterns of time-averaged velocity vectors,<V> and streamline, <Ψ> topology for angle of attack of α=10° for yaw angles of 0°≤ θ ≤15° are presented in Figure 4. On the first column of Figure 4 shows that the velocity vectors have relatively high magnitude on both sides of the mid-chord axis, but along the leading edges on both sides the magnitude of velocity become very small.The symmetrical flow topology can be seen in the case of zero yaw angle. However, farther outboard from the plane of symmetry, the magnitude of velocity becomes relatively small for all cases of yaw angle. At all values of yaw angle the magnitude of velocity vectors,<V> show an abrupt decrease immediately downstream of the leading edge. Furthermore, a well-defined swirl pattern of velocity is evident in the near region of the apex as seen in all images of the first column of Figure 4. This swirl pattern gets larger as angle of attack, α is increased. In the central portion of each of these swirl patterns, the magnitude of velocity vectors,<V> is very small. Examining the all experimental results, the region of low velocity also covers the whole surface of the wing, when angle of attack is increased. For instance, the low velocity region dominates the whole surface of the delta wing at attack angle α=17°.

On the second column of Figure 4, the time-averaged streamline patterns, <Ψ> are presented. In the case of zero yaw angle, a pair of well defined foci which is designated as F_1 and F_2 are developed near region of the apex over the wing surface as seen in the first image. Two positive bifurcation lines, L^+ which demonstrates the divergency of streamlines toward the single line are observed inboard of each vortex whereas negative bifurcation lines, L^- which represents the merging of all streamlines into single line formed along the leading edge. In addition, two saddle points are taken place on negative bifurcation lines, L^- close to the trailing edge of the delta wing. Examining the all experiments,it can be seen that the flow structure close to the wing surface is sensitive to the variation of yaw angle.

While yaw angle is applied to the delta wing, the symmetry of the flow topology is deteriorated. Generally, the streamline pattern, <Ψ>, tends to be linear through its lengthwise direction at the leeward side of the delta wing. Because of this reason, focus, F, located at this side begins to disappear. However, diameter of the focus located at windward side is increased as the yaw angle is increased. This situation causes the large low velocity region at windward side of the delta wing, but it is not the case for the other side. So that, effect of yaw angle does not cause any significant difference in size between the two separated flow regions for the yaw angle in the range of 0°≤θ≤6°.

b. Patterns of Time-Averaged Vorticity Contours

The patterns of time-averaged vorticity, <ω> for angle of attack of α=10° for yaw angles of 0°≤ θ ≤15° are shown in Figure 5. To be able to make direct comparison, for the contours of time-averaged vorticity, <ω> minimum and incremental values was taken same values as $[<\omega>]_{min}$ =0.4 s^{-1} and $\Delta[<\omega>]$ =1 s^{-1}, respectively. When yaw angle is increased, values of the contours of time-averaged vorticity, <ω> decrease on the leeward side of the wing due to the movement of vortex breakdown location downstream of the trailing edge of the wing, on the other hand this values, <ω> are constant on the winward side of the wing. As seen in Figure 5, there is a pair of well-defined clusters of negative and positive time-averaged vorticity, <ω> represented as M which emanates from the leading edge of the delta wing. Along the side edges of the wing elongated vortices occur represented as L_R and L_E.

c. Patterns of Transverse and Streamwise Velocity Components

Patterns of time-averaged component of transverse velocity, <v>/U for various yaw angles and angle of attack α=10° shown in the first column of Figure 6. The contours are represented by negative and positive <v>/U. The positive and negative contours are demonstrated by solid and dashed lines, respectively. To be able to make a direct comparison between the minimum and incremental values of contours of time-averaged component of transverse velocity kept constant. The values of minimum and incremental values are $[<v>/U]_{min}$ =0.03 s^{-1} and $\Delta[<v>/U]$ =0.03 s^{-1}. There are two well-defined clusters of main positive and negative contours at both side of the delta wing chord axis. There is a symmetrical structure under delta wing surface in the case of zero yaw angle. While the delta wing is under effect of yaw angle, the distribution of <v>/U contours changes. Examining all images, the contours have an elongated form starting from leading edge of the delta wing . Also, there is a pair of contours at immediately downstream of the delta wing apex. They widen along the leading edge of delta wing and get stronger while angle of attack increases. The extrema of positive and negative contours move further downstream on the free-stream flow direction while yaw angle is increased at angle of attack α=10°. The main positively rotated contours do not unite with the positively rotated secondary contours located at immediately downstream of the delta wing apex, for angle of attack α=10° and yaw angle θ=15°. Patterns of time-averaged component of transverse velocity, <u>/U for various yaw angles and angle of attack α=10° shown in the second column of Figure 6.

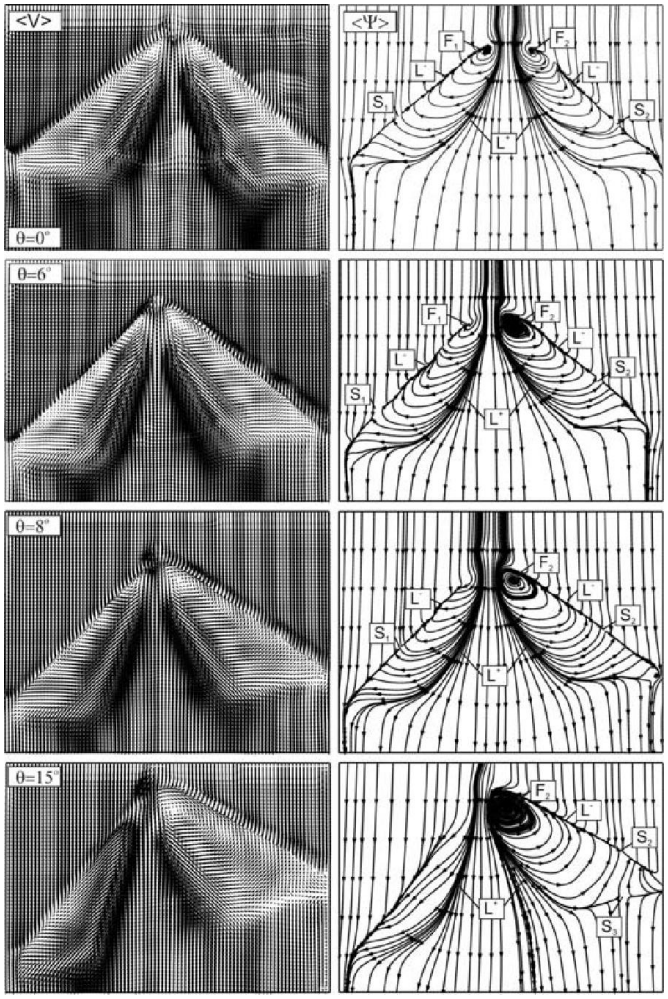

Figure 4 Patterns of streamline, <Ψ> and time-averaged vorticity, <V> for angle of attack of $\alpha=10^{o}$

The positive and negative contours are demonstrated by solid and dashed lines, respectively. The minimum and incremental values of contours of dimensionless streamwise velocity, <u>/U and transverse velocity, <v>/U components for all yaw angles were kept constant for better comparison between the time-averaged velocity components The vortex breakdown occurs closer to the apex on the windward side of the wing and other vortex breakdown occurs close to the trailing edge on the leeward side of the wing as seen from the dye visualization results. However, it is remarkable that this discernible alteration of the onset of vortex breakdown seems to have significant influence on the patterns of <u>/U and <v>/U even in the near surface of the wing.

As seen in the first image of the contours of streamwise time-averaged velocity component, <u>/U, a negative velocity distributions take place on both side edges of the wing. The domain of the negative velocities, <u>/U gets smaller in size when the yaw angle, θ of the wing increases at the windward side. As seen in Figure 6, negative velocity component is disappeared on the leeward side at θ=15°.

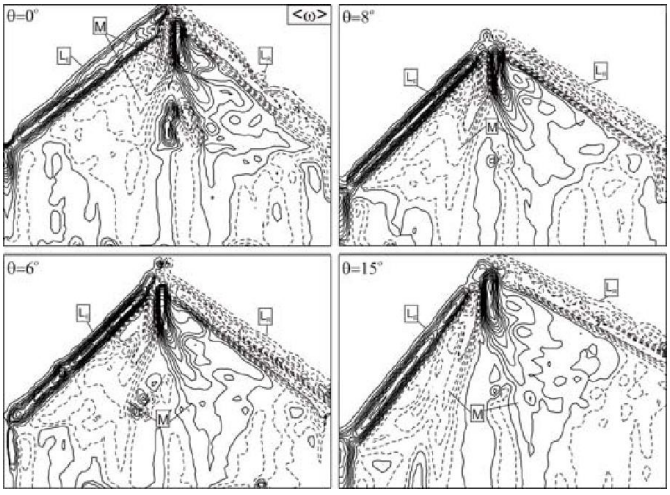

Figure 5 Patterns of time-averaged vorticity,ω contours for angle of attack of $\alpha=10^{o}$. Minimum and incremental values are $[<\omega>]_{min}=0.4\ s^{-1}$ and $\Delta[<\omega>]=1\ s^{-1}$

d. Patterns of Reynolds Stress Correlations

Reynolds stress correlations, $<u'v'>/U^2$ normalized by free-stream velocity, U are shown in Figure 7. The positive and negative contours are demonstrated by solid and dashed lines, respectively. To be able to make a direct comparison between the minimum and incremental values of contours of time-averaged component of transverse velocity kept constant. The values of minimum and incremental values are $[<u'v'>/U^2]_{min}=0.00075$, $\Delta[<u'v'>/U^2]=0.00075$. Although images were taken in close proximity to the surface of the wing, the structure of vortex breakdown has a considerable effect on the wake region. The concentration of Reynolds-stress distributions $<u'v'>/U^2$ occupy a wider region on windward side and have a higher values comparing to the leeward side of the wing when yaw angle is increased. The strength of $<u'v'>/U^2$ are attenuated and central point of the extreme moves further downstream in the flow direction when the yaw angle is increased.

CONCLUSION

The present study observes on formation and development of leading edge vortices and vortex breakdown. Also, wing/vortex interaction can be seen from present results. These phenomena are investigated both qualitatively and quantitatively using dye visualization and the Particle Image Velocimetry (PIV) technique. The wing has a leading edge sweep angle of $\Lambda=40^{o}$ and the changes in the flow structure are obtained by varying yaw angle of the delta wing within the range of $0^{o}\leq\theta\leq15^{o}$ for angle of attack $\alpha=10^{o}$. There is a symmetrical flow structure on the delta wing in the case of zero yaw angle. Also, there is a coherent pair of leading edge vortices starting from the apex of the delta wing. When the delta wing is under the effect of a yaw angle the symmetrical flow structure deteriorates and a vortex breakdown occurs earlier on the windward side of the delta wing compared with the leeward side.

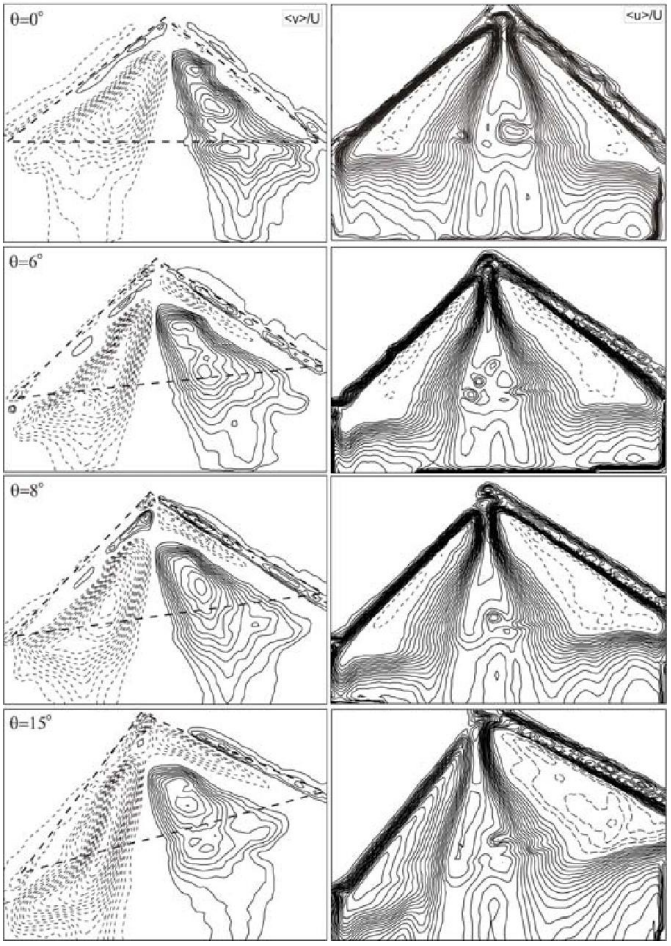

Figure 6 Patterns of time-averaged components of streamwise, [<u>/U] and transverse, [<v>/U] velocity for the angle of attack $\alpha=10^o$. Minimum and incremental values are $[<v>/U]_{min}$ =0.03 s^{-1}, Δ[<v>/U] =0.03 s^{-1} and [<u>/U]=0.05, Δ[<u>/U] =0.05

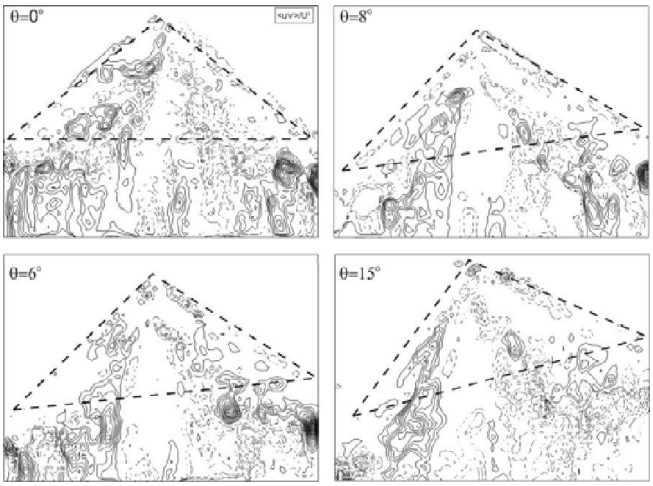

Figure 7. Patterns of time-averaged turbulent Reynolds stress components for angle of attack $\alpha=10^o$, minimum and incremental values are $[<u'v'>/U^2]_{min}$=0.00075, $\Delta[<u'v'>/U^2]$=0.00075

ACKNOWLEDGEMENTS

The authors acknowledge the financial support of The Scientific and Technological Research Council of Turkey (TUBITAK) for funding under project No: 105M225.

REFERENCES

[1] Delery, J. M., "Aspects of Vortex Breakdown", *Progress in Aerospace Sciences*, Vol. 30, pp. 1-59, 1994.

[2] Yaniktepe, B., and Rockwell, D., "Flow Structure on a Delta Wing of Low Sweep Angle" *AIAA Journal*, Vol. 42, No. 3,2004.

[3] Yaniktepe B. And Rockwell D., "Flow Structure on Diamond and Lambda Planforms:Trailing-Edge Region" *AIAA Journal*, Vol. 43, No. 7, 2005.

[4] Yavuz, M., Elkhoury, M., and Rockwell, D., "Near-Surface Topology and Flow Structure on a Delta Wing", *AIAA Journal*, Vol. 42, No. 2, 2004, pp. 332-340.

[5] Ol, M. V., and Gharib "Leading-Edge Vortex Structure of Nonslender Delta Wings at Low Reynolds Number" *AIAA Journal*, Vol. 41, No. 1, 2003.

[6] Elkhoury, M. and Rockwell, D., "Visualized Vortices on Unmanned Combat Air Vehicles Planform: Effect of Reynolds Number." *Journal of Aircraft*, Vol. 41, No. 5, pp. 1244-1246, 2004.

[7] Taylor, G.S., Gursul, I., "Buffeting flows over a low-sweep delta wing.", *AIAA Journal*, Vol. 42, No. 9, 2004.

[8] Gursul, I., Gordnier, R. and Visbal, M., "Unsteady aerodynamics of nonslender delta wings", Progress in Aerospace Sciences 41, pp.515–557 2005.

[9] Elkhoury, M., Yavuz, M. M. and Rockwell, D., "Near-Surface Topology of a Unmanned Combat Air Vehicles Planform: Reynolds Number Dependence", *Journal of Aircraft*, Vol. 42, No. 5, September/October, 2005, 1318-1330, 2005.

[10] Goruney, T., Rockwell, D., "Flow Past a Delta Wing with a Sinusoidal Leading Edge: Near-Surface Topology and Flow Structure", *Experiments in Fluids*, Vol. 47, pp. 321–331, 2009.

[11] Sohn, M. H., and Lee, K. Y., "Experimental Investigation of Vortex Flow of a Yawed Delta Wing Having Leading Edge Extension," *20th AIAA Applied Aerodynamics Conference*, 24-26 June 2002, St. Louis, Missouri.

[12] Sohn, M. H., and Lee, K. Y., "Effects of Sideslip on the High-Incidence Vortical Flow of a Delta Wing with the Leading Edge Extension," *41st Aerospace Sciences Meeting and Exhibit*, 6-9 January 2003, Reno, Nevada.

[13] Ki Young Lee, Myong Hwan Sohn, "The Vortical Flow Field of Delta Wing with Leading Edge Extension", *KSME International Journal*, Vol. 17 No. 6, 2003

[14] Sohn, M. H., Lee, K. Y., And Chang, J. W., Vortex Flow Visualization of a Yawed Delta Wing with Leading-Edge Extension", *Journal of Aircraft*, Vol. 41, No. 2, 2004.

[15]Canpolat, C., Yayla, S., Sahin, B., and Akilli, H., "Dye Visualization of the Flow Structure over a Yawed Nonslender Delta Wing", *Journal of Aircraft,* Vol.46, No.5, 2009.

[16]Prasad A. K. Stereoscopic particle image velocimetry, *Experiments in Fluids*, Vol. 29, No. 2 , 2000.

[17]Adrian, R. J., "Twenty Years of Particle Image Velocimetry", *Experimental Fluids*, Vol. 39, pp. 159–169, 2005.

[18] Raffel M., Willert C.E., Wereley S.T. and Kompenhans J. "Particle Image Velocimetry: A Practical Guide", *Springer-Verlag*, 1998.